Transition to limit cycle oscillations in fluid-structure interactions: a time-series approach to study causal dependencies*

Sombuddha Bagchi[†] and Vishnu R. Unni[‡] and Abhishek Saha[§]
Department of Mechanical and Aerospace Engineering, University of California San Diego, La Jolla, CA 92093, USA

We investigate the dynamical characteristics corresponding to the structural fluctuations of a cantilever suspended in a turbulent flow. To investigate the intricate dynamics of the flow-structure interaction, first, we explore the ability of network analysis to identify the different dynamical states and probe the viability of using quantifiers of network topology as precursors for the onset of limit cycle oscillations. By increasing the Reynolds number, we observe that the structural oscillations, measured using a strain gauge, transition from low amplitude chaotic oscillations to large amplitude periodic oscillations associated with limit cycle oscillations. We characterize the dynamical states of the system by constructing the weighted correlation network from the time series of strain and identifying the network properties which have the potential to be used as precursors for the onset of limit cycle oscillations. Furthermore, we use Pearson correlation to illustrate the evolution of mutual statistical influence between the structural oscillations and the flow field. We use this information and the Granger causality to identify the causal dependence between the structural oscillations and velocity fluctuations. By identifying the causal variable during each regime, we illustrate the directional dependence through a 'cause-effect' relationship in this flow-structure interaction as it transitions to limit cycle oscillations.

I. Introduction

We encounter fluid flow over solid structures in many natural and industrial processes. The interaction between flows and an elastic structure, commonly known as flow-structure interaction, can lead to aeroelastic instabilities, which can cause significant damage to bridges and buildings [1]. Aeroelastic instabilities can also cause dangerous oscillations of lift generating structures of an aircraft during the flight, which may compromise the flight's safety and stability, leading to loss of life and property. [2, 3]. Although researchers have conducted many fundamental and applied studies on this topic [4], identifying the onset of such instabilities remains challenging.

In the early 20th century, Hunsaker [5] and Perring[6] performed fundamental research on aeroelastic instability. The development of finite element analysis in the 1970s paved the way for advanced analysis of aeroelastic instability on complex surfaces [7, 8]. Some essential methods, such as the flutter margin method [9]; Nissim and Gilyard method [10]; non-iterative P-K method [11]; and multi-fidelity modeling [12], are popular in anticipating the onset of aeroelastic instability or sustained limit cycle oscillations. However, such methods cannot fully capture the non-linearities arising from, e.g., structural fatigue and flow non-uniformities which can only be incorporated by real-time analysis of the time series of an appropriate parameter.

The temporal evolution of system variables can provide us with detailed insights into the system's dynamics. Dynamical systems analysis, or the analysis of systems evolving in time subject to various constraints, can help us obtain information about the states of the system [13–15]. In several studies, dynamical systems analysis for fluid-structure interactions, particularly in turbulent flow, have been performed, and newer insights have been formed[16–20]. Researchers have acknowledged that most dynamical systems in nature are, in fact, complex systems. The "complexity" of a complex system stems from the difficulty in inferring the system's behavior from its properties. Ignoring or dismissing such intricate system behavior as noise during modeling would lead to inaccuracies in the model. Characterizing such problems is domain-specific as there is no general theory for addressing these intricacies, and they must be tackled

^{*}Presented at the AIAA SciTech Forum 2022, January 3-7, 2022, San Diego, CA (Paper # AIAA2022-0353

[†]Graduate Research Assistant, AIAA Student Member

[‡]Currently Assistant Professor, Indian Institute of Technology Hyderabad, India

[§] Assistant Professor, Senior Member of AIAA, email: asaha@eng.ucsd.edu

case by case. Therefore, researchers in complex systems generally tend to these problems by focusing on capturing rather than reducing the complexity of the systems [21, 22]. Systems are generally considered complex if there are intricate interactions between a large number of their constituent subsystems, where we cannot anticipate the emergent phenomena arising due to this mutual interaction from the behavior of individual component subsystems [23, 24]. Thus, we can use different tools from dynamical systems theory like recurrence plots to provide accurate descriptions of the different states of the system [25]. In some scenarios, we can analyze a complex system by using the complex network theory tools [26, 27]. For instance, we can study the temporal evolution of a dynamic state variable of a complex system by analyzing the evolution of the topology of a complex network derived from the time series of the state variable. One method of deriving complex networks from a time series involves considering different data points of the time series as individual nodes of the network, and connecting these nodes using edges that represent some relationship between the two data points, such as correlations and causal relations. There are numerous ways to derive complex networks from a time series and the construction methodology determines the type of information extracted from the time series which are embedded in the network properties. For instance, some complex networks like correlation networks constructed using Pearson correlation coefficients can provide information regarding the statistical interrelationships from climate data on both local and global scales [28].

In addition to analysis of structural aspects, a separate treatment of the interaction of the flow and the structure is required to elaborate on the change in dynamics as the system transitions to instability. The interaction of the vortex shedding with the structure can lead to vortex-induced vibrations. The vortex shedding frequency locks into the structure's natural frequency, therefore leading to sustained high amplitude periodic oscillations [29]. The vortex shedding due to an elastically mounted rigid cylinder has been well-documented [30–32]. The lock-in response of a flat plate is nearly identical to the response of a standard airfoil, which indicates that a surface with a single sharp edge can simulate the lock-in characteristics of an airfoil shaped structure [33]. [34] performed experimental investigations on flow around a flat plate placed normal to the stream and constrained to rotate perpendicular to the axial and transverse direction of the flow. The range of the forcing frequencies of the plate was kept in the neighborhood of the natural vortex shedding frequencies for a range of Reynolds number. They observed that with an increase of forcing frequency amplitude, the amplitude of peak corresponding to vortex shedding frequency from spectra of wake velocity reduces. There is an emergence of peak corresponding to the forcing frequency, which dominates during the lock-on regime. [35] studied the torsional oscillations due to vortex-induced oscillations occur when the natural frequency of structure, the vortex shedding frequency from the vibrating body and the frequency of the vibrating body in freestream are similar.

Due to the emergence of synchronous behavior during the transition to instability, analysis of correlations between multiple variables can provide crucial insights into how the different variables mutually interact [36]. However, correlations can only provide information on whether and how much these variables are statistically interlinked but cannot express the causal relationship between them. Therefore, in addition to obtaining how these variables are correlated, it is interesting to elucidate the causal dependence between them [37], which we cannot obtain from correlation information. Determination of this causal relationship is crucial in control systems analysis, where feedback is provided to the 'cause' in order to obtain a desired response [38]. We note that the Granger causality, introduced by Clive Granger [39], is one of the earliest and well-established statistical methods to determine and quantify the causal relationship between various time series. Granger causality tells us that a signal y_t causes x_t if a signal x_t can be better predicted by including past terms of y_t . Granger causality has been used to analyze turbulent channel flows to obtain the various causalities between streak breakdown and wall-normal activities [40].

With the overarching goal of identifying the underlying relationship between the dynamics of the flow and the structure oscillations during the transition to limit cycle oscillations, in this study, we will use three different yet relevant analyses of time series data. First, we construct a weighted correlation network [41] from the time series of strain resulting from the interaction between a cantilever and turbulent flow. Subsequently, we characterize the different dynamical states of the system by using various network properties that quantify different aspects of the network based on its topological features. Multiple network properties are studied, and we identify and communicate those which can adequately classify the different states. Furthermore, we study the underlying relationship between the flow and structure oscillations by obtaining the causal relationship between them. To obtain the causalities between the structural oscillations and velocity fluctuations, first, we obtain information about how the velocity field and strain are mutually interlinked statistically. Then, we use Granger causality to illustrate the changes in causal dependency as the flow transitions towards the limit cycle oscillations.

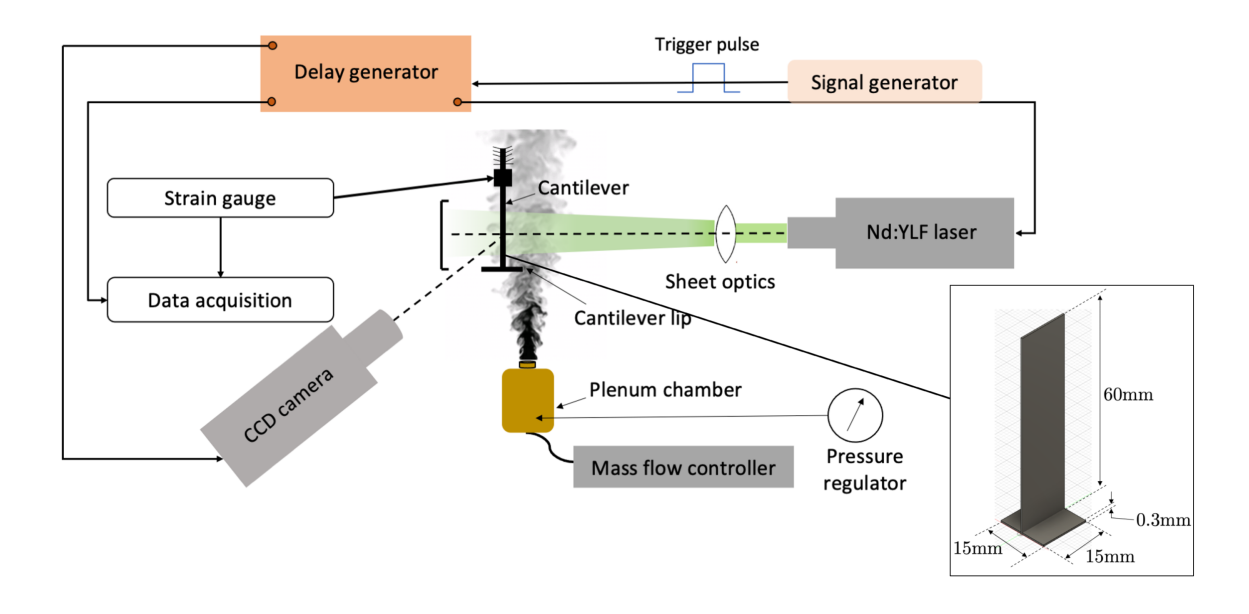


Fig. 1 Schematic of experimental setup with magnified image of the cantilever inset (not drawn to scale).

II. Experimental setup and sample time series

We used a simple setup to conduct the experiments where a cantilever was suspended in a turbulent flow resulting in flow-structure interaction (Fig. 1). We generate the turbulent jet by discharging compressed air through a cylindrical nozzle, with diameter D = 16mm, which impacts the cantilever asymmetrically. Alicat mass flow controller controlled the flow rate of the compressed air to modulate the mean velocity of the jet, which in turn allowed changes in the dynamical states of the structure [42, 43]. The cantilever beam (Elastic modulus = 1.37GPa) has a length of 60mm, a width of 15mm, and a thickness of 0.3mm, and was anchored at one end. We kept the relative position of the flow and the structure constant. The lower end of the cantilever has a small horizontal fin of 15mm attached to it. The experimentally obtained natural frequency of the structure was observed to be 12.5Hz (see supplementary material). The impact of the jet on the cantilever causes oscillations in the structure. We measure the strain on the cantilever arising due to this flow structure interaction using a strain gauge mounted just below the fixed end of the cantilever. We used a strain gauge of bridge resistances $350\Omega \pm 0.6\%$ and gauge factor $2.130 \pm 0.5\%$ attached to one arm of a Wheatstone bridge connected to an input voltage of 12V. To obtain information about the interaction of the turbulent jet with the cantilever, we perform particle image velocimetry (PIV). A laser sheet emanating from an Nd-YLF laser (527nm) passes through the jet's center and the cantilever. Seeding the flow by DEHS droplets resulted in scattering the laser light by these particles, a phenomenon called Mie scattering, which we captured using a high-speed Phantom v710 camera with a 24-70mm lens situated at a right angle to the laser sheet. We used a signal generator and an external delay generator to obtain the PIV and strain data simultaneously at a sampling frequency of 2kHz. We obtain the normalized velocity field fluctuations, $Z_v = (v - \bar{v})/\sigma_v$, from the PIV by dividing it by its standard deviations, where v, \bar{v} and σ_v are the instantaneous value, mean, and standard deviation of the axial velocity component, respectively. We observe similar fluctuations in the transverse direction velocity as well.

We performed the experiment by varying in the incoming airflow rate Q from 5 slpm to 70 slpm, corresponding to a flow Reynolds number Re = 1100 - 8100 ($Re = (\rho U_{mean}D)/\mu_g$, where ρ is the density of air $\approx 1.2kg/m^3$, U_{mean} is mean velocity of the turbulent jet, D is the diameter of nozzle and μ_g is the dynamic viscosity of air $\approx 1.85 \times 10^{-5} \text{Pa-s}$), quasi-steadily resulting in transition from aperiodic low-amplitude structural oscillations to the periodic instability through the intermittency route. The system approaches periodic oscillatory behavior around Re = 7000. The aperiodic low amplitude oscillations are chaotic, which is confirmed by the 0-1 test for chaotic system [44]. The Z-values of time series of strain fluctuations ($Z_s = \frac{s-\mu}{\sigma}$, where μ and σ are mean and standard deviation of strain fluctuations respectively)

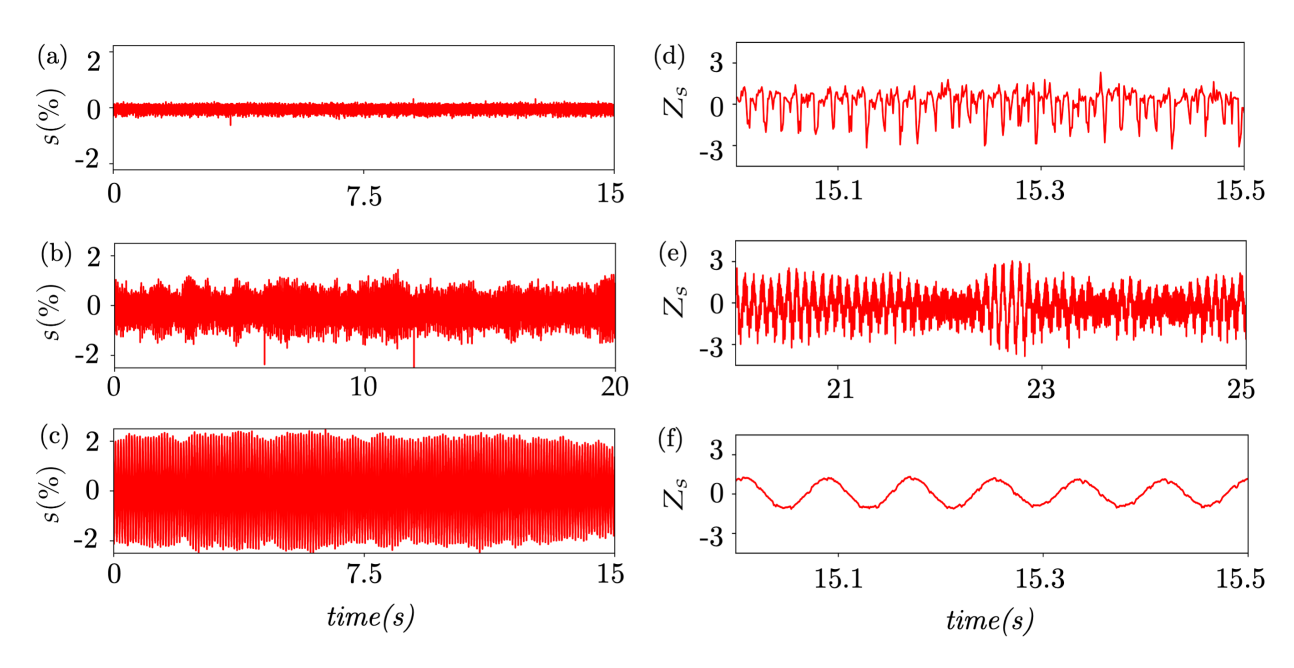


Fig. 2 Strain time series zoomed out (left column) and normalized zoomed in (right column) views. (a, d) chaotic regime (Re = 2300); (b, e) intermittency regime (Re = 5800); (c, f) periodic regime (Re = 8100).

are illustrated for different dynamical states in Fig. 2. The three dynamical states investigated are namely: chaotic regime (CR), intermittency regime (IR), and periodic regime (PR) [45]. As we travel from chaos to periodicity through intermittency, the oscillations become more periodic. The corresponding instantaneous vorticity $(1/s)[\omega = \frac{\partial v}{\partial x} - \frac{\partial u}{\partial y}]$, where u and v are velocity components in the x and y directions respectively obtained from the PIV images for the three dynamical regimes of the surrounding flow field is illustrated in Fig. 3. We note that the strength of the vorticity increases with an increase in Re. In other words, as the system transits to limit cycle oscillations or periodic oscillation, the flow field demonstrates a strong vorticity field. During this regime, the ensuing interaction of the flow and the structure results in vortex shedding from the lip with a frequency of 12.6Hz (see supplementary material). We can observe the location of the shear layer from the vorticity field (marked with black dotted lines in Fig. 3) where a strong vorticity field is present. This zone contains strong velocity gradients. We will now define four strategically located points on the flow-field (as shown in Fig. 3), at which we will perform Granger causality analysis (Section III.C) to evaluate the degree of interaction between the flow and cantilever. These four points are as follows, Point A: upstream of the lip of the cantilever; Point B: right of the lip of the cantilever; Point C: downstream of the lip of the cantilever; Point D: far downstream in the wake of the cantilever.

III. Results and discussions

This section will use the following methods to analyze the time-series data obtained from flow structure interactions. First, to characterize the transition of the system to limit cycle oscillations, we will use the correlation network using time series of strain imposed on the structure during the transition to instability. Such temporal characterization of structural oscillations which delineate a distinct increase with change in parameter has the potential to be used as precursors to instability. Subsequently, we will evaluate the correlation between flow velocity and strain on the structure to evaluate their influence on each other. Finally, we evaluate the cause-effect relation using Granger causality.

A. Weighted correlation network with embedding: temporal characterization of dynamical regimes

This paper discusses a complex network framework that brings out the correlations and mutual statistical similarity between different parts of a dynamical system's trajectory obtained from the time series. Here, the connectivity between various network components doesn't necessarily imply 'physical' vertices and edges but instead reflects the statistical interrelationships between the dynamics showcased by the system under observation [46]. In this network, the vertices and edges reflect the correlations between the various subsets of the time series. In general, auto-correlation measures

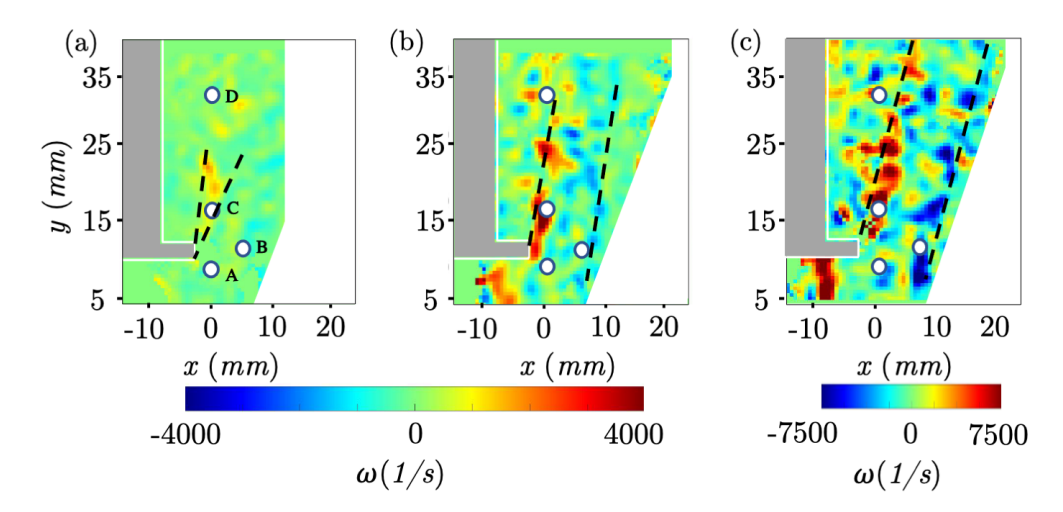


Fig. 3 Instantaneous vorticity field at (a) chaotic regime (Re = 2300), (b) intermittency regime (Re = 5800), (c) periodic regime (Re = 8100). Dotted lines mark strong shear layer regions. A,B,C & D are 4 representative points to be discussed in Section III.C

the linear relationship between lagged values of a time series and thus can help us detect the seasonality or periodicity of the time series. Since auto-correlation provides a quantitative estimate of periodicity in the time series, we propose a weighted correlation network with embedding (CN) built using the correlation properties of a time series $\phi(t)$ of length N. The first step of proper network representation for a time series is to provide an algorithm to define the vertices and edges depending on what information we want to extract from the time series. The next step is to determine the proper measures to characterize the system's dynamics from the rich toolbox of complex network topological quantifiers. These quantifiers help capture the dynamic system's various features, which cannot be obtained from conventional time series analyses. As we construct the complex networks from time series, these networks have specific signatures corresponding to the dynamical regimes they belong to. Since the response data of the structure correspond to the state it is currently in, e.g., high amplitude periodic oscillations which are usually associated with aeroelastic instability or limit cycle oscillations, we can determine the relative state of the system by comparing it with the completely periodic sinusoidal oscillations. We normalize the time series by their standard deviations to be comparable with the response from any other measurement data for, e.g., turbulence excitation of wings or control surface excitation if the system goes through a similar intermittent route to instability. Therefore, the main limitation of CN quantifiers is that these can be used as potential precursors to the onset of any adverse event if that system takes a similar route to instability.

To construct the CN, we first need to transform the scalar time series into a multivariate state space, which is performed using Takens' embedding theorem [47]. It is often used to perform a time delay embedding for state space reconstruction of time series. To obtain the delayed time vectors, we use a delayed time set $[\phi(i), \phi(i+\tau), ..., \phi(i+(m-1)\tau)]$ of length m, where m is the embedding dimension and τ is the delay, is taken. The dimension m is obtained from False Nearest Neighbour Method [48] and the delay is obtained from the first minimum of mutual information vs. delay plot. It obtains the time-delayed coordinates of the state space, which are maximally statistically independent of each other as possible (a concept similar to getting the basis functions of a coordinate system). Therefore, the strain at present and later time is a non-linear combination of almost all the dynamic variables of a system, since between $\phi(i)$ and $\phi(i+\tau)$, enough time would have evolved for the system to produce new information in the state space. So, mutual information collected in this network answers the particular question: in our time series, how much can one learn about the strain experienced by the structure at τ samples later, by measuring the strain at present [49]. Average mutual information is given by the expression:

$$[I(\phi(t), \phi(t+\tau)) = \sum_{i,j} p_{ij}(\tau) log \frac{p_{ij}(\tau)}{p_i p_j}]$$
(1)

Where p_i is the probability of $\phi(t)$ lying in the bin i of histogram constructed from scalar ϕ , $p_{ij}(\tau)$ probability of $\phi(t)$ lying in bin i and, $\phi(i+\tau)$ in bin j. Further details regarding the application of this methodology can be obtained

from [50]. The first minimum of the I vs delay plot is the delay τ . After obtaining the delayed vectors, we create a matrix translating this set by one time-step over the whole series resulting in a $N - (m-1)\tau \times m$ matrix, whose ith row element is

 $x_i = \begin{bmatrix} \phi(i) & \phi(i+\tau) & \dots & \phi(i+(m-1)\tau) \end{bmatrix}$ where $i = 1, 2, \dots, N - (m-1)\tau$ (2)

and N is the length of the time series. In the present study, we construct the network from 2000 data points or N = 2000. Now we find the correlation of each row, x_i , with every other row, x_j , (including itself) according to the Pearson correlation coefficient $r_{i,j}$:

$$r_{i,j} = r(x_i, x_j) = \frac{\sum_{k=1}^{m} (x_i(k) - \bar{x_i})(x_j(k) - \bar{x_j})}{\sqrt{\sum_{k=1}^{m} (x_i(k) - \bar{x_i})^2} \sqrt{\sum_{k=1}^{m} (x_j(k) - \bar{x_j})^2}}$$
(3)

where $\bar{x_i} = \sum_{k=1}^{m} x_i(k)/m$. Thus, a weighted adjacency matrix w_{ij} is created after subtracting the identity matrix from the correlation matrix $r_{i,j}$,

$$w_{ij} = r_{ij} - \delta_{ij},\tag{4}$$

where δ is an identity matrix. In the present study, we keep the positive values of the correlation matrix unchanged while we take the negative values as zero. This network preserves the topology of the attractor, i.e., the network structures maintain the geometry of the state space. For example, chaotic attractors have fractal topology, while intermittent and periodic orbits have orbits in the shape of a torus with different degrees of roundness [45]. This change in topology and therefore the preservation of the state space topology is observed in CN structures in Figure 4. The network can also find correlations between elements at both short and longer time scales.

In this network, the delay vectors preserve the non-linear correlations between two sets of time series, and the weighted correlation matrix removes the ambiguity of selecting a critical correlation coefficient. The smaller but meaningful correlations are not lost, which would have been the case if we had used a binary adjacency matrix. The network structures of different regimes are shown in Fig. 4. We visualize the network structures in Gephi network visualization software [51], and ForceAtlas 2 is the algorithm that has been used to create the structures. ForceAtlas 2 is a force-directed layout where the nodes repulse each other, and the edges attract the nodes (similar to springs); their strength depends on the nodal degree and the distance between the nodes. Additionally, the edge weights also affect the interactions in this weighted network. The sum of all these interactions leads to a converged state. Further detailed discussion regarding the layout is provided in [52]. The chaotic attractor is shown in Fig. 4a. We observe some symmetry, regularity, and non-uniformity in the network due to short-term correlations that occur because of its deterministic nature. Such small correlations might have been lost if a binary adjacency matrix had been used. As we transition towards limit cycle oscillations, the network becomes more ordered and uniform. In Fig. 4c, for limit cycle oscillations, there is a uniform distribution of nodes all over the network in the annular disc (torus in 3-dimensional phase space).

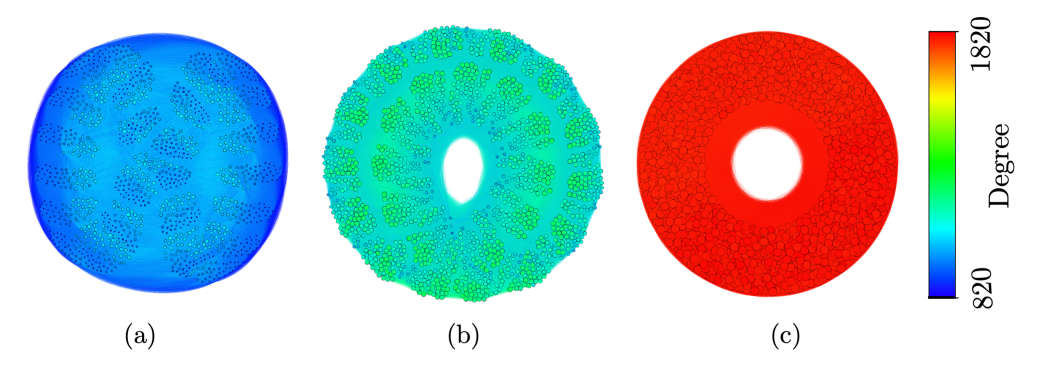


Fig. 4 Weighted correlation network structures of s' at different regimes. (a) chaotic regime (Re = 2300), (b) intermittency regime (Re = 5800), (c) periodic regime (Re = 8100).

To quantitatively characterize the various topological aspects of the network, one can use various quantification measures, whose values are expected to evolve with the variation in the dynamical states of the system. In the present

study, we only describe those quantifiers which has the potential to forewarn onset of instability. The first quantifier is the weighted Characteristic Path Length (CPL_w) , which is the mean of all the shortest possible weighted paths between the nodes of a network. For a network of total number of nodes N, the normalized Characteristic Path Length can be mathematically expressed as $CPL_w^* = \sum_{i \neq j} w_{ij} d_{ij} / (N(N-1))$, where d_{ij} is the shortest possible path between node i and j and j and j is the corresponding weight of that path. The second quantifier is the average weighted degree $(\langle k_w \rangle)$, which is defined as the mean of the number of possible weighted connections for each node of a network over the whole network. Mathematically, it can be expressed as $\langle k_w \rangle = \sum_{i \neq j} w_{ij} / N$. Finally, the average betweenness centrality $(C_b(n))$ measures how a node lies on the path between other nodes. The nodes with high betweenness influence the network considerably because they control the connectivity between the different nodes of a network. Mathematically, betweenness centrality is defined as $C_b(n) = \sum\limits_{i,j\neq n}^N \hat{\sigma}_{i,j}(n)/\hat{\sigma}_{i,j}$ where, $\hat{\sigma}_{i,j}$ is the number of shortest paths between nodes i and j and $\hat{\sigma}_{i,j}(n)$ is the number of shortest paths between nodes i and j which passes through the node n. To simplify visualization, we normalize each quantifier (denoted by *) by dividing their corresponding values by the value of the quantifier for the sinusoidal time series.

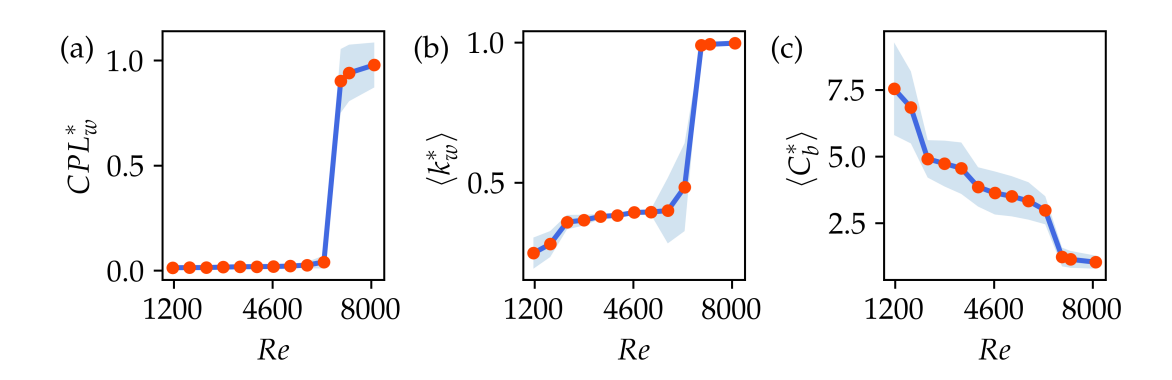


Fig. 5 Network properties of weighted correlation network.(a) Variation of CPL_w^* with Re. (b) Variation of $\langle k_w^* \rangle$ with Re. (c) Variation of $\langle C_b^* \rangle$ with Re.

The evolution of these network quantifiers for CN with Reynolds number (Re) is illustrated in Fig. 5. The quantification measures of CN are highly dependent upon the correlation in state-space between the different subsets of the whole time series. As the Re crosses a critical value (Re > 7000) required for the onset of limit cycle oscillations, the characteristic path length, CPL_w^* , sharply increases to a higher value. This dramatic change is due to more correlations in the periodic regime, resulting in an increased number of connections in the network. Since these connections are weighted by the correlations as observed from the network structures in Fig. 4, the mean path length is larger for each connection occurring due to the correlation in states in the time series. Next, we focus on the degree of a node, which represents the node's connectivity. The variation of average degree $(\langle k_w^* \rangle)$ with Re in Fig. 5b shows a sudden increase as limit cycle oscillations is initiated for (Re > 7000). We note that the correlation between different states increases substantially with an increase in periodicity in the flow-structure interaction system. In a periodic regime, there is higher synchronicity or connectivity between the nodes than the chaotic attractor, which is reflected in increased $\langle k_w^* \rangle$. The third quantifier, betweenness centrality, gives information about regions with a low nodal density that separates the regions of a high nodal density in a network. For periodic data, there will be a uniform distribution of the regions with a high nodal density since the correlations in time series occur at regular intervals, unlike the chaotic regime, where the correlations are not so uniformly distributed. In chaotic attractors, the presence of nodes that monopolizes the ties between low nodal density and high nodal density (also known as geometric bottlenecks) results in a larger number of nodes with higher connectivities [53]. Hence, betweenness centrality is larger for chaotic regime and low for periodic regime (high Re) as seen in Fig. 5c.

In summary, we can see that quantification measures of a correlation network constructed from strain data in an aeroelastic system show drastic changes at the onset of instability or periodic oscillations. These markers, thus, has the potential to be used as precursors to instability and therefore, can be the subject of detailed study in future. Now that we obtained information about the temporal correlations of strain data from the cantilever, we focus on how there is a statistical linkage between the flow to structural oscillations and vice versa in both temporal and spatial dimensions. The

goal is to develop a causal relationship between the flow dynamics and the cantilever. To do this, first, we investigate the statistical correlations between velocity and structural fluctuations.

B. Evolution of bi-variate correlations

In the context of flow-structure interaction, we can use multivariate correlations to extract information on how correlations between the structure and fluid flow evolve with time. Although such a correlation cannot show if there is a cause-effect relationship between two variables, it can provide us an idea of whether the mutual influence between the variables is strong enough to perform prediction-based statistical analysis on them. Obtaining this correlation is, indeed, the first step in assessing the *cause-effect* relationship between variables.

To perform correlation analysis, we use the Pearson correlation between Z_v and Z_s , the normalized velocity, and strain fluctuations, respectively (defined in Section II). This approach aims to observe the evolution of the correlations between velocity and strain, calculated at multiple sub-periods, with time. The length of the sub-period is n = 40, larger than the minimum sample size for Pearson correlation given by David [54] and Bonnet et al [55]. For n samples, the correlation is given by,

$$r(Z_{v}, Z_{s}) = \frac{\sum_{k=1}^{n} (Z_{v(i)}(k) - \bar{Z}_{v})(Z_{s(i)}(k) - \bar{Z}_{s})}{\sqrt{\sum_{k=1}^{n} (Z_{v(i)}(k) - \bar{Z}_{v})^{2}} \sqrt{\sum_{k=1}^{n} (Z_{s(i)}(k) - \bar{Z}_{s})^{2}}}$$
(5)

where, \bar{Z}_v and \bar{Z}_s is the mean of normalized velocity and strain fluctuations respectively.

We illustrate the results of this analysis for the three dynamical regimes in Fig. 6a-c. For chaotic regime (CR), we observe that the correlation is weak for almost all the instances. The weak correlation is because the interaction between the turbulent flow field and the aperiodic oscillations of the cantilever is uncorrelated in time. Since there is very little statistical influence between the fluctuations in the turbulent flow and the cantilever fluctuations, we observe very low values of $r(Z_v, Z_s)$ in Fig. 6a.

As we increase the Re, the vorticity at the shear layer start to become stronger, as illustrated in Fig. 3b. As the bar starts oscillating with a higher amplitude, the fluctuations near that region start oscillating in tandem with the cantilever. With an increase in flow rate or Re, there is an increase in periodic bursts interspersed with chaotic fluctuations, which is known as intermittency. We illustrate the variation of correlation with the position of the bar in Fig. 6b. Although $r(Z_v, Z_s)$ for other parts of the flow field varies with time, there is substantial and mostly consistent either high positive or high negative $r(Z_v, Z_s)$ along with the shear layer. The high $r(Z_v, Z_s)$ is primarily because the shear layer near the lip oscillates periodically due to the movement of the bar.

Moreover, the influence of oscillations of the cantilever on the flow is maximum at the lip because it is the point of maximum deflection. Vortex shedding occurs in the wake of the cantilever lip at a frequency different from cantilever oscillations. At this Re, the perturbations produced by vortex shedding and structural oscillation near the wake of the lip are unable to reach the state of resonance, a behavior also observed for other geometries of flow-structure interactions [56].

With a further increase in Re, the system reaches the state of limit cycle oscillations. During this periodic state, the vortex shedding due to the movement of the bar causes the bar to oscillate in the transverse direction to the mean flow. At this stage, the strong influence of vortex shedding emerges as the shedding frequency, and frequency of the oscillation in the cantilever becomes similar[57] as shown in Fig. 7. This results in higher magnitude of the correlation between Z_s and Z_v , a phenomenon known as 'lock-in' [58] and shown in Fig. 6c. Similar lock-in phenomena between the frequency of buffeting flow and of an elastically suspended airfoil has also been observed in aeroelastic systems [59]. Lock-in between acoustic pressure and heat release fluctuations has also been observed in thermoacoustic systems [60] during combustion instability. During periodic regime (PR), there are large-amplitude periodic oscillations of the cantilever and the flow field. The shear layer is positively correlated with the bar and the vortex shedding causing them to oscillate simultaneously during the upwards trajectory of the cantilever.

We can use the information about the extent of mutual statistical correlation between the different regions' flow and the cantilever to develop a cause-effect relationship between the individual oscillators. While causation implies correlation, the observed correlation does not warrant causation. Thus, in the following section, we will explore the viability of using Granger causality, a well-established statistical hypothesis test, to see if causality exists in an aeroelastic system that transitions to limit cycle oscillations.

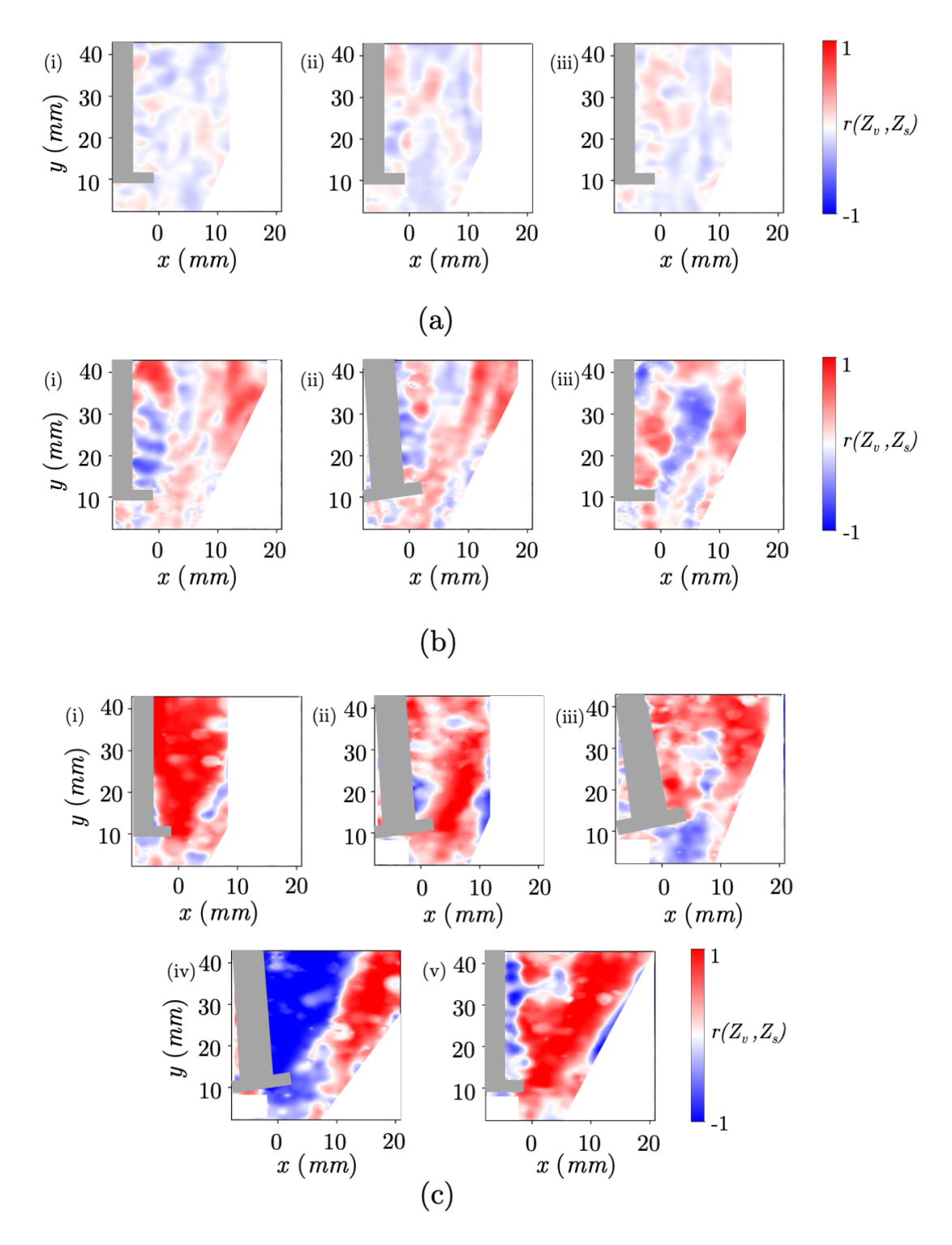


Fig. 6 Variation of correlation between Z_v and Z_s with movement of the cantilever at (a) chaotic regime (Re = 2300), (b) intermittency regime (Re = 5800), (c) periodic regime (Re = 8100).

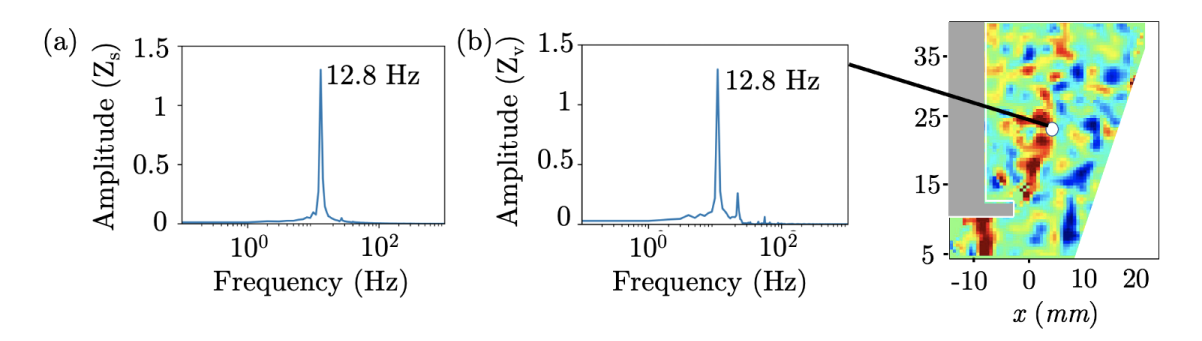


Fig. 7 FFT of (a) normalized strain and (b) normalized velocity fluctuations during limit cycle oscillations (position of probe in the flow marked in the corresponding vorticity field).

C. Causal dependencies between flow and structure

Next, we focus on the directional dependence or the causalities between different variables. Among many methods, we can quantify this dependence using Granger causality [39]. It is, indeed, one of the earliest and most well-established statistical methods to determine and quantify the causal relationship between various time series. The method verifies if inclusion of past observations of the 'cause' y(t) in the linear regression model comprising of x(t) and y(t) reduces the error in predicting the 'effect' x(t). If this condition is satisfied, the method concludes that the time series x(t) is Granger caused by y(t) (both stationary in time). Therefore, Granger causality provides a statistical measure of how the change in one time series can be used to predict the change in another time series in the future.

To perform this analysis, first, we provide a univariate linear autoregression model for time series x(t) with lag τ , which is less than the length of the time series N,

$$x(t_m) = \sum_{i=1}^{\tau} p_i x(t_{m-i}) + \epsilon_1(t_m)$$
 (6)

and a bi-variate linear regression model which can be expressed as,

$$x(t_m) = \sum_{i=1}^{\tau_x} \tilde{p}_i x(t_{m-i}) + \sum_{j=1}^{\tau_y} \tilde{q}_j y(t_{m-j}) + \epsilon_2(t_m)$$
 (7)

In equations 6 and 7, p_i , \tilde{p}_i and \tilde{q}_i are the coefficients of the model while ϵ_1 and ϵ_2 are their respective prediction errors. The lags τ_x and τ_y are obtained using Bayesian Information Criterion (BIC) [61]. In order to conclude whether y(t) causes x(t), the coefficient \tilde{q}_i must be significantly different than 0. This is determined by performing the residual sum of squares based F-test of the null hypothesis that $\tilde{q}_i = 0$. The F-test can be expressed as:

$$F = \frac{RSS_u - RSS_l/\tau_y}{RSS_l/(T - \tau_y - \tau_x - 1)} \sim F(\tau_y, T - \tau_y - \tau_x - 1)$$
(8)

where, RSS_u denotes the residual sum of squares without lagged times series $y(t_m)$, and RSS_l denotes the residual sum of squares with lagged times series $y(t_m)$. If $F(\tau_y, T - \tau_y - \tau_x - 1)$ is less than the corresponding F_α from the F-table, we reject the null hypothesis. We have used a significance level of $\alpha = 0.05$ in the present study, i.e., if there is more than 95% probability that $\tilde{q}_i \neq 0$, we conclude that y(t) Granger causes x(t). Keeping lower significance levels might prevent the identification of the causal variable, commonly known as Type II error in statistics, while larger significance levels can lead to spurious causalities.

The current study tries to obtain the causal relationship between velocity fluctuations and strain fluctuations. We use the method outlined by Jiang et al. [62] to procure information about the evolving causal dependencies in the system. However, since the motivation of the current study is to identify the most influential causal dependencies, we look at the probability of occurrence of each of the possible causalities. In this method, we obtain the time series of flow velocity fluctuations (Z_v) from points A, B, C, and D in the flow field (illustrated in Fig. 3) and the time series of strain fluctuations (Z_s) of length T, both normalized by their respective standard deviations. Then, for each of the larger time series, we create a smaller sub-period of length n_t . The criteria for choosing this sub-period are as follows: (1) the time

series for each sub-period must be stationary, (2) the length of the sub-period should be sufficient to provide information about the various short-term transitions, and (3) the causal dependencies should not mirror the larger time series. Once we fix the sub-period size using the above criteria, we slide this sub-period of constant length by a single time step over the whole time series, therefore obtaining information about the evolution of causal dependencies at each time interval. In the current study, there are only four possibilities of causality: (1) velocity causes strain $(v \to s)$, (2) strain causes velocity $(s \to v)$, (3) both strain and velocity cause each other $(v \leftrightarrow s)$ and (4) none of the variable cause each other $(v \times s)$. Here, $v \times s$ denotes that we can ascertain no significant causal dependencies between the variables. For bidirectional causality $(v \leftrightarrow s)$, the implications here are two-fold: either both the time series are indeed causal to each other, or there is a presence of one or more common causal processes mutually driving both the time series [63]. A further investigation will be required to differentiate between such causalities, which is beyond the focus of the present study.

We perform Granger analysis for these four representative points in the flow and illustrate the individual probabilities of occurrence of these four possible causalities in Fig. 8. For CR, as also outlined in Section III.B, there is no region with any strong directional dependence between velocity and strain which we have illustrated in Fig. 8a. This low dependence is reasonably intuitive since the correlations between the movement of the cantilever and the turbulent velocity fluctuations are very weak. Therefore, it is difficult to identify a causal variable that can help predict the other dependent variable. Points A and B are perturbed weakly by the movement of the cantilever. Even though the correlations are weak, the causality analysis is sensitive to the chaotic structural oscillations and their effect on the flow. That is why we observe an increase in the probability of both $(s \to v)$ and $(v \to s)$ in point C, located just downstream of the lip. At point C, as observed from Fig. 3a, there is a strong velocity gradient due to the presence of the shear layer, which increases the directional dependence between v and s. Point D in the flow is too far away from the lip or shear layer to be affected by the cantilever's oscillations. Therefore, we observe no significant contribution from $(s \to v)$ and $(v \to s)$.

At a higher Re and in the IR state, there is slowly an emergence of causal dependence in the flow adjacent to the cantilever (Points A, B, and C). Here, we observe that there is an increase in the probability of strain Granger causing velocity $(s \to v)$ in this region in Fig. 8b. Since the effect of the structural oscillations is most potent along the path of oscillation of the cantilever, point B shows the highest probability of $(s \to v)$, while at A and C, it is marginally lesser. Higher correlations in this region, as also observed in Section III.B, is consistent with the fact that the high amplitude oscillations of the cantilever cause the intermittent velocity fluctuations to originate, resulting in the emergence of order in the flow field, i.e., correlated shear layer oscillations and vortex shedding. The movement of the cantilever essentially controls the vortex shedding process in this regime, as the oscillation frequency approaches the natural frequency of the cantilever. The mutual dependence between flow and velocity $(v \leftrightarrow s)$ increases as we move downstream. This increased dependence can be because the vortex shedding frequency is different from the natural frequency of the cantilever. There is a mutual causality between them, i.e., the structural oscillations affect the vortex shedding, which affects the cantilever's movement. Both are causing each other as large-scale perturbations due to the structural oscillations and vortex shedding occurring at different frequencies, neither of which are phase-locked.

As an even higher Re, when we reach the PR state, the high amplitude fluctuations of the shear layer and the vortex shedding is driving the periodic oscillations of the cantilever, and hence at all locations (A, B, C, and D), we observe high probability for velocity Granger causing strain $(v \to s)$, as shown in Fig. 8c. During this regime, the vortex shedding frequency escalates to the oscillating frequency of the cantilever [64]. It is to be noted that since there is a broadband spectrum due to the high turbulence (see supplementary material), the structure's natural frequency is one of the many peak frequencies present in the turbulent flow. Despite this, the vortex shedding frequency locks on to this particular frequency having a strong amplitude as we increase the Re (in our case, the natural frequency of 12.5Hz) resulting in sustained high amplitude oscillations. Here, the flow regime constantly feeds energy to the cantilever during each cycle of oscillations, resulting in instability-induced and sustained high amplitude cantilever oscillations. The momentum to the cantilever resulting in high amplitude oscillations is imparted by the turbulent jet (therefore, the Granger causal dependence) itself, which has a large momentum of its own. Therefore, the resultant vortex-shedding phenomenon and the turbulent jet itself cause the cantilever to oscillate at high amplitude at its natural frequency. We observe the considerable influence of the high amplitude oscillations of the cantilever on flow (Probability of $s \rightarrow v$ is ≈ 0.15) at A, B, and C, since they are located near the highly oscillating lip of the cantilever. In the wake of the cantilever, far downstream at D, the influence of the cantilever is minimized. Therefore, there is a decrease in the probability of $s \to v$. A similar response has also been observed in the case of a circular cylinder in a fluid flow by Bishop [65].

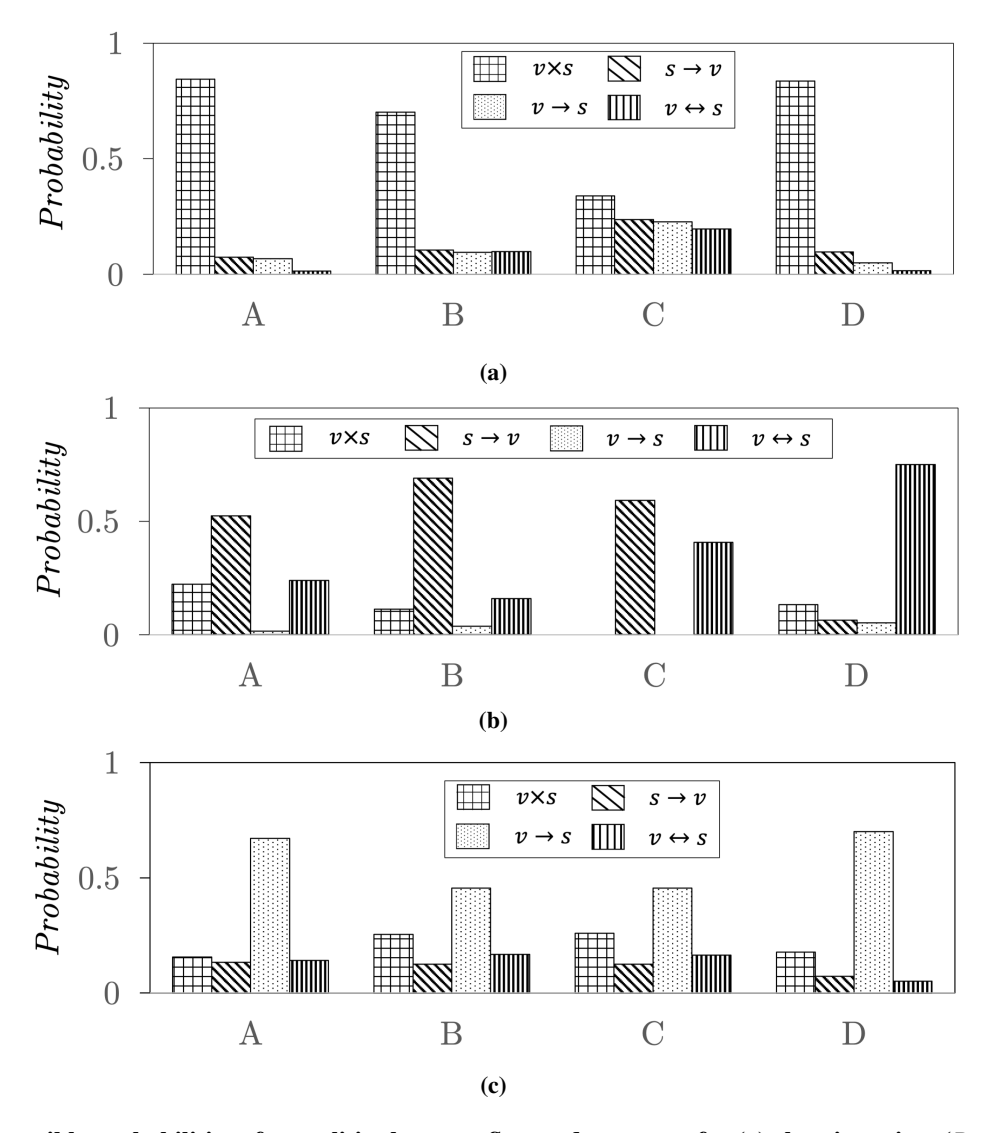


Fig. 8 All possible probabilities of causalities between flow and structure for (a) chaotic regime (Re = 2300), (b) intermittency regime (Re = 5800), (c) periodic regime (Re = 8100). Probabilities are illustrated for the 4 points marked in Fig. 3.

IV. Summary and Conclusions

The current investigation has illustrated how we can use time series-based methods to provide precursors to the onset of limit cycle oscillations. By mapping the temporally fluctuating strain into a complex network framework, we have used various quantification parameters that can quantify the topological aspects of the complex network as potential precursors to instability. These quantifiers capture the transition of the dynamical system, in our case, the oscillating cantilever, from aperiodic to sustained periodic oscillations. Each precursor illustrated in this study has its merits and specific purpose. As we approach limit cycle oscillations, each quantifier varies with a different level of sensitivity and robustness. The characteristic path length and average degree vary rapidly after intermittency, while the betweenness centrality varies less drastically. Therefore, one can use multiple quantifiers in combination with each other to provide a reliable set of precursors for the onset of the limit cycle oscillations that prevents false positive and false negative warnings or even a single one based on specific requirements of the system.

To illustrate the causal dependence between the flow and the cantilever, we first obtain the mutual statistical correlation between the variables through the bivariate Pearson correlation for the whole flow field. For the chaotic regime, we observe very little statistical correlation between the variable as the structural oscillations are chaotic, and there is not much influence on the turbulent fluctuations by the cantilever. We observe a stronger correlation between

intermittency and periodic regime as order emerges in the flow structure interaction system. There is a strong positive correlation along the shear layer due to the correlated movement of the cantilever and the flow field. Once we obtain the statistical extent of mutual correlation between the variables, we try to determine the directional dependence between them. For the chaotic regime, due to a low statistical correlation between v and s, we cannot obtain a clear causal dependence between them. However, fluctuations in the regions in the flow near the cantilever lip are affected by the movement of the cantilever. With the emergence of order during intermittency, we observe that the structural oscillations cause velocity fluctuations in the vicinity of the lip of the cantilever. Further downstream, there is mutual causality due to the effect of vortex shedding and high amplitude oscillations of the cantilever. Further increase in Re results in limit cycle oscillations when the periodic vortex shedding and shear layer oscillations lock onto the transverse movement of the cantilever. The large momentum of the turbulent jet and the vortex shedding ensuing due to the interaction causes the sustained high amplitude oscillations of the cantilever at its natural frequency. This combined system oscillates at the oscillation frequency of the cantilever.

Acknowledgements

This work was supported, in parts, by the US-National Science Foundation, Grant Number (CBET-2053671) and the internal grants from the Jacobs School of Engineering at UCSD.

References

- [1] Matsumoto, M., Shirato, H., Yagi, T., Shijo, R., Eguchi, A., and Tamaki, H., "Effects of aerodynamic interferences between heaving and torsional vibration of bridge decks: the case of Tacoma Narrows Bridge," *J. Wind Eng. Ind. Aerod.*, Vol. 91, No. 12-15, 2003, pp. 1547–1557.
- [2] Garrick, I. E., and Reed, W. H., "Historical development of aircraft flutter," *J. Aircraft*, Vol. 18, No. 11, 1981, pp. 897–912. https://doi.org/10.2514/3.57579.
- [3] Hill, G., "Advances in aircraft structural design," Proc Third Anglo-American Conference, Vol. 1, 1951.
- [4] Iovnovich, M., Nahom, T., Presman, M., Avsaid, D., Braier, T., and Raveh, D. E., "Assessment of advanced flutter flight-test techniques and flutter boundary prediction methods," *Journal of Aircraft*, Vol. 55, No. 5, 2018, pp. 1877–1889.
- [5] Hunsaker, J., and Wilson, E. B., "Report on Behavior of Aeroplanes in Gusts," 1917.
- [6] Perring, W., Wing flutter experiments upon a model of a single seater biplane, HM Stationery Office, 1928.
- [7] Dowell, E. H., "Panel flutter A review of the aeroelastic stability of plates and shells," *AIAA Journal*, Vol. 8, No. 3, 1970, pp. 385–399. https://doi.org/10.2514/3.5680.
- [8] Olson, M. D., "Some flutter solutions using finite elements," *AIAA Journal*, Vol. 8, No. 4, 1970, pp. 747–752. https://doi.org/10.2514/3.5751.
- [9] Zimmerman, N. H., and Weissenburger, J. T., "Prediction of flutter onset speed based on flight testing at subcritical speeds," *Journal of Aircraft*, Vol. 1, No. 4, 1964, pp. 190–202. https://doi.org/10.2514/3.43581.
- [10] Nissim, E., and Gilyard, G. B., "Method for experimental determination of flutter speed by parameter identification," 30th Structures, Structural Dynamics and Materials Conference, 1989, p. 1324.
- [11] Pitt, D., "A new non-iterative PK match point flutter solution," 40th Structures, Structural Dynamics, and Materials Conference and Exhibit, 1999, p. 1353.
- [12] Thelen, A. S., Leifsson, L. T., and Beran, P. S., "Aeroelastic Flutter Prediction using Multi-fidelity Modeling of the Aerodynamic Influence Coefficients," *AIAA Scitech 2019 Forum*, 2019, p. 0609.
- [13] Landman, M. J., "Time-dependent helical waves in rotating pipe flow," Journal of fluid mechanics, Vol. 221, 1990, pp. 289–310.
- [14] Seshadri, A., Pavithran, I., Unni, V. R., and Sujith, R., "Predicting the amplitude of limit-cycle oscillations in thermoacoustic systems with vortex shedding," *AIAA Journal*, Vol. 56, No. 9, 2018, pp. 3507–3514.
- [15] Weng, Y., Unni, V. R., Sujith, R., and Saha, A., "Synchronization framework for modeling transition to thermoacoustic instability in laminar combustors," *Nonlinear Dynamics*, Vol. 100, No. 4, 2020, pp. 3295–3306.

- [16] Dowell, E. H., "Nonlinear oscillations of a fluttering plate. II." AIAA journal, Vol. 5, No. 10, 1967, pp. 1856–1862.
- [17] Paolucci, S., and Chenoweth, D. R., "Transition to chaos in a differentially heated vertical cavity," *Journal of Fluid Mechanics*, Vol. 201, 1989, pp. 379–410.
- [18] Guzman, A., and Amon, C., "Transition to chaos in converging–diverging channel flows: Ruelle–Takens–Newhouse scenario," *Physics of Fluids*, Vol. 6, No. 6, 1994, pp. 1994–2002.
- [19] Corke, T., and Knasiak, K., "Stationary travelling cross-flow mode interactions on a rotating disk," *Journal of Fluid Mechanics*, Vol. 355, 1998, pp. 285–315.
- [20] He, S., Jonsson, E., Mader, C. A., and Martins, J. R., "Coupled Newton–Krylov Time-Spectral Solver for Flutter and Limit Cycle Oscillation Prediction," *AIAA Journal*, Vol. 59, No. 6, 2021, pp. 2214–2232.
- [21] Boccara, N., and Boccara, N., Modeling complex systems, Vol. 1, Springer, 2004.
- [22] Sterman, J. D., "Learning in and about complex systems," System dynamics review, Vol. 10, No. 2-3, 1994, pp. 291–330.
- [23] Ottino, J. M., "Engineering complex systems," Nature, Vol. 427, No. 6973, 2004, pp. 399-399.
- [24] Ladyman, J., Lambert, J., and Wiesner, K., "What is a complex system?" *European Journal for Philosophy of Science*, Vol. 3, No. 1, 2013, pp. 33–67.
- [25] Eckmann, J. P., Oliffson Kamphorst, O., and Ruelle, D., "Recurrence plots of dynamical systems," Epl, Vol. 4, No. 9, 1987, pp. 973–977. https://doi.org/10.1209/0295-5075/4/9/004.
- [26] Strogatz, S. H., "Exploring complex networks," *Nature*, Vol. 410, No. 6825, 2001, pp. 268–276. https://doi.org/10.1038/35065725, URL https://doi.org/10.1038/35065725.
- [27] Strogatz, S. H., "Exploring complex networks," nature, Vol. 410, No. 6825, 2001, pp. 268–276.
- [28] Donges, J. F., Zou, Y., Marwan, N., and Kurths, J., "Complex networks in climate dynamics," *The European Physical Journal Special Topics*, Vol. 174, No. 1, 2009, pp. 157–179.
- [29] Besem, F. M., Kamrass, J. D., Thomas, J. P., Tang, D., and Kielb, R. E., "Vortex-induced vibration and frequency lock-in of an airfoil at high angles of attack," *Journal of Fluids Engineering*, Vol. 138, No. 1, 2016.
- [30] Sarpkaya, T., "Vortex-induced oscillations: a selective review," 1979.
- [31] Williamson, C. H., Govardhan, R., et al., "Vortex-induced vibrations," *Annual review of fluid mechanics*, Vol. 36, No. 1, 2004, pp. 413–455.
- [32] Williamson, C., and Govardhan, R., "A brief review of recent results in vortex-induced vibrations," *Journal of Wind engineering and industrial Aerodynamics*, Vol. 96, No. 6-7, 2008, pp. 713–735.
- [33] Ehrmann, R., Loftin, K., Johnson, S., and White, E., "Lock-In of Elastically Mounted Airfoils at High Angles of Attack," 50th AIAA Aerospace Sciences Meeting including the New Horizons Forum and Aerospace Exposition, 2012, p. 1209.
- [34] CHEN, J., and FANG, Y.-C., "LOCK-ON OF VORTEX SHEDDING DUE TO ROTATIONAL OSCILLATIONS OF A FLAT PLATE IN A UNIFORM STREAM," *Journal of Fluids and Structures*, Vol. 12, No. 6, 1998, pp. 779–798. https://doi.org/https://doi.org/10.1006/jfls.1998.0164, URL https://www.sciencedirect.com/science/article/pii/S0889974698901645.
- [35] Yang, Y., and Strganac, T. W., "Experiments of vortex-induced torsional oscillation of a flat plate in cross flow," *AIAA journal*, Vol. 51, No. 6, 2013, pp. 1522–1526.
- [36] Li, Z., Zhang, Z., Wang, J., and Yang, J., "Pressure–heat flux correlations for shock interactions on v-shaped blunt leading edges," AIAA Journal, Vol. 57, No. 10, 2019, pp. 4588–4592.
- [37] Omata, N., and Tsutsumi, S., "Causal Analysis of Flowfields Using Clustering Entropy," AIAA Journal, Vol. 58, No. 12, 2020, pp. 5472–5477.
- [38] Garg, A., and Tangirala, A. K., "Metrics for interaction assessment in multivariable control systems using directional analysis," *Industrial & Engineering Chemistry Research*, Vol. 57, No. 3, 2018, pp. 967–979.
- [39] Granger, C., "Economic processes involving feedback," Information and Control, Vol. 6, No. 1, 1963, pp. 28–48. https://doi.org/ https://doi.org/10.1016/S0019-9958(63)90092-5, URL https://www.sciencedirect.com/science/article/pii/S0019995863900925.

- [40] Tissot, G., Lozano-Durán, A., Cordier, L., Jiménez, J., and Noack, B. R., "Granger causality in wall-bounded turbulence," *Journal of Physics: Conference Series*, Vol. 506, IOP Publishing, 2014, p. 012006.
- [41] Yang, Y., and Yang, H., "Complex network-based time series analysis," *Physica A: Statistical Mechanics and its Applications*, Vol. 387, No. 5-6, 2008, pp. 1381–1386.
- [42] Pavithran, I., Unni, V. R., Varghese, A. J., Premraj, D., Sujith, R., Vijayan, C., Saha, A., Marwan, N., and Kurths, J., "Universality in spectral condensation," *Scientific reports*, Vol. 10, No. 1, 2020, pp. 1–8.
- [43] Pavithran, I., Unni, V. R., Varghese, A. J., Sujith, R., Saha, A., Marwan, N., and Kurths, J., "Universality in the emergence of oscillatory instabilities in turbulent flows," EPL (Europhysics Letters), Vol. 129, No. 2, 2020, p. 24004.
- [44] Gottwald, G. A., and Melbourne, I., "A new test for chaos in deterministic systems," *Proceedings of the Royal Society of London. Series A: Mathematical, Physical and Engineering Sciences*, Vol. 460, No. 2042, 2004, pp. 603–611.
- [45] Strogatz, S. H., Nonlinear dynamics and chaos with student solutions manual: With applications to physics, biology, chemistry, and engineering, CRC press, 2018.
- [46] Zou, Y., Donner, R. V., Marwan, N., Donges, J. F., and Kurths, J., "Complex network approaches to nonlinear time series analysis," *Physics Reports*, Vol. 787, 2019, pp. 1–97.
- [47] Takens, F., "Lect. Notes in Math,", 1981.
- [48] Kennel, M. B., Brown, R., and Abarbanel, H. D., "Determining embedding dimension for phase-space reconstruction using a geometrical construction," *Physical review A*, Vol. 45, No. 6, 1992, p. 3403.
- [49] Abarbanel, H., Analysis of observed chaotic data, Springer Science & Business Media, 2012.
- [50] Fraser, A. M., and Swinney, H. L., "Independent coordinates for strange attractors from mutual information," *Physical review A*, Vol. 33, No. 2, 1986, p. 1134.
- [51] Bastian, M., Heymann, S., and Jacomy, M., "Gephi: an open source software for exploring and manipulating networks," *Proceedings of the international AAAI conference on web and social media*, Vol. 3, 2009, pp. 361–362.
- [52] Jacomy, M., Venturini, T., Heymann, S., and Bastian, M., "ForceAtlas2, a continuous graph layout algorithm for handy network visualization designed for the Gephi software," *PloS one*, Vol. 9, No. 6, 2014, p. e98679.
- [53] Zhang, J., Sun, J., Luo, X., Zhang, K., Nakamura, T., and Small, M., "Characterizing pseudoperiodic time series through the complex network approach," *Physica D: Nonlinear Phenomena*, Vol. 237, No. 22, 2008, pp. 2856–2865.
- [54] David, F. N., *Tables of the ordinates and probability integral of the distribution of the correlation coefficient in small samples*, Cambridge University Press, 1938.
- [55] Bonett, D. G., and Wright, T. A., "Sample size requirements for estimating Pearson, Kendall and Spearman correlations," *Psychometrika*, Vol. 65, No. 1, 2000, pp. 23–28.
- [56] Baek, S.-J., and Sung, H. J., "Quasi-periodicity in the wake of a rotationally oscillating cylinder," *Journal of Fluid Mechanics*, Vol. 408, 2000, pp. 275–300.
- [57] Bearman, P. W., "Vortex shedding from oscillating bluff bodies," *Annual review of fluid mechanics*, Vol. 16, No. 1, 1984, pp. 195–222.
- [58] Griffin, O. M., and Hall, M. S., "Review—Vortex Shedding Lock-on and Flow Control in Bluff Body Wakes," *Journal of Fluids Engineering*, Vol. 113, No. 4, 1991, pp. 526–537. https://doi.org/10.1115/1.2926511, URL https://doi.org/10.1115/1.2926511.
- [59] Raveh, D. E., and Dowell, E. H., "Aeroelastic responses of elastically suspended airfoil systems in transonic buffeting flows," *AIAA journal*, Vol. 52, No. 5, 2014, pp. 926–934.
- [60] Pawar, S. A., Mondal, S., George, N. B., and Sujith, R., "Temporal and spatiotemporal analyses of synchronization transition in a swirl-stabilized combustor," *AIAA Journal*, Vol. 57, No. 2, 2019, pp. 836–847.
- [61] Schwarz, G., "Estimating the dimension of a model," The annals of statistics, 1978, pp. 461-464.
- [62] Jiang, M., Gao, X., An, H., Li, H., and Sun, B., "Reconstructing complex network for characterizing the time-varying causality evolution behavior of multivariate time series," *Scientific reports*, Vol. 7, No. 1, 2017, pp. 1–12.

- [63] Chen, P., and Hsiao, C.-Y., "Looking behind Granger causality," 2010.
- [64] Meskell, C., and Pellegrino, A., "Vortex shedding lock-in due to pitching oscillation of a wind turbine blade section at high angles of attack," *International Journal of Aerospace Engineering*, Vol. 2019, 2019.
- [65] Bishop, R. E. D., and Hassan, A., "The lift and drag forces on a circular cylinder oscillating in a flowing fluid," *Proceedings of the Royal Society of London. Series A. Mathematical and Physical Sciences*, Vol. 277, No. 1368, 1964, pp. 51–75.